THE EUROPEAN SOCIETY OF MEDICINE
Medical Research Archives, Volume 13 Issue 11

RESEARCH ARTICLE

Simplified MR Neurography Protocol for Pudendal Neuropathy Using a 1.5-Tesla Magnet and Black Blood sequence: Technique, Grading system and Validation

Vittorio Piloni[1], Marco Fogante[2], Tiziana Manisco[3]

[1]Diagnostic Imaging Center Affidea Iniziativa Medica, via Rialto 14, 35043 Monselice (Padua), Italy - ORCID 0000 0003 2447 3825
[2]Department of Radiology, Maternal-Child, Senological, Cardiological Radiology and Outpatient Ultrasound, University Hospital of Marche, 60126 Ancona, Italy - ORCID 0000 0003 2993 5718
[3]Diagnostic Imaging Center "Diagnostica Marche" Osimo Stazione, via industria 1 60027 Ancona, Italy - ORCID 0000 0003 2328 9364

OPEN ACCESS

PUBLISHED
30 November 2025

CITATION
Piloni, V., et al., 2025. Simplified MR Neurography Protocol for Pudendal Neuropathy Using a 1.5-Tesla Magnet and Black Blood sequence: Technique, Grading system and Validation. Medical Research Archives, [online] 13(11). https://doi.org/10.18103/mra.v13i11.7031

DOI
https://doi.org/10.18103/mra.v13i11.7031

ISSN
2375-1924

ABSTRACT

Background: Pudendal neuropathy diagnosis currently relies on advanced MR neurography using 3-Tesla magnets, 3D imaging, and contrast enhancement. Despite these innovations, diagnostic accuracy remains uncertain.

Purpose: To validate a simplified MR imaging protocol and grading system for pudendal nerve damage using a conventional 1.5-Tesla magnet without contrast.

Materials and Methods: We retrospectively analyzed 100 consecutive patients (60 females, 40 males; mean age: 48 years, 95% CI: 45.1–50.9) with suspected pudendal neuropathy (Nantes criteria) examined between January and May 2024. MR neurography was performed using a 1.5-T horizontal magnet and phased-array coil in two phases: (1) T2-weighted turbo spin echo sequences in multiple planes; (2) proton density SPAIR sequences with fat and flow suppression. Two blinded radiologists independently assessed signal hyperintensity in Alcock's canal using a 0–3 brightness scale. Discrepancies were resolved by a third expert. Inter- and intra-observer agreement was calculated via weighted kappa (WK).

Results: Of 87 frames with abnormalities, 13 were grade 0, 33 grade 1, 37 grade 2, and 17 grade 3. Intra-observer agreement was excellent (WK = 0.875 and 0.920), and inter-observer agreement was high (WK = 0.78). Observer 3 resolved 30 discrepancies, mostly minor (27 cases with one-point difference). Major discordance occurred in only 3 cases.

Conclusion: This simplified, contrast-free MR protocol using a 1.5-T magnet shows high reliability even among non-specialized readers and may offer a practical tool for pudendal neuropathy assessment, especially in resource-limited settings.

Keywords: MR neurography; Pudendal neuralgia; Alcock canal; Black Blood pulse sequences; Entrapment neuropathies.

Introduction

Peripheral nerve entrapment syndromes are frequently attributed to mechanical or dynamic compression of a nerve segment within anatomically constrained regions such as osteofibrous tunnels, fibrous apertures, or passageways adjacent to ligaments or muscles. These structural bottlenecks can compromise neural function, leading to a spectrum of clinical manifestations. Although neurological examination and electrophysiological studies remain the cornerstone of diagnostic evaluation, advanced imaging modalities — including high-resolution ultrasound and magnetic resonance (MR) neurography — have emerged as valuable adjuncts. They not only assist in localizing the site and identifying the underlying etiology of nerve compression, but also play a critical role in excluding alternative pathologies that may contribute to the patient's symptoms.

In particular, MR neurography of the pelvic nerves is increasingly considered by clinicians and researchers in the evaluation of patients with complex chronic pelvic pain syndromes. These conditions pose significant diagnostic challenges due to their multifactorial etiology, often involving gynecologic, urologic, neurologic, and intestinal systems. Once interstitial cystitis, endometriosis, solitary rectal ulcer, and anoperineal abscess have been ruled out as potential causes, clinical attention must shift toward the possibility of a peripheral neuropathy as the underlying source of pain. This diagnostic rationale has been a key driver of imaging research efforts in this domain, particularly over the past two decades.

Since its initial introduction in 1992 and subsequent reports[1–5], it has become evident that visualizing peripheral nerves in the pelvis is more difficult than in other regions of the body. This is due to several adverse factors, including small nerve size, long and tortuous course, anatomical variations, and the presence of obscuring structures such as hollow viscera with physiologically variable contents.

Currently, there is general consensus[6–9] that the diagnostic cornerstones of MR neurography include: (1) optimal depiction of the cross-sectional and longitudinal architecture of pelvic nerves; and (2) use of selective nerve pulse sequences to detect signal changes, swelling, and fascicular architecture alterations. Although the role of paramagnetic contrast agents remains controversial, combining fluid-sensitive sequences with double fat and vascular suppression is considered essential. This approach is further enhanced by high-resolution 3T magnet systems and selective 3D multiplanar nerve-targeted sequences for nerve pathway reconstruction[10–12]. However, these technical requirements and the expertise needed for accurate image interpretation are not universally available.

This study aims to: (a) describe the technical details of an MR neurography protocol for visualizing the pudendal nerve within Alcock's canal using a conventional 1.5T scanner without contrast agent administration; and (b) introduce and validate a visual three-point grading scale for assessing pudendal nerve injury severity.

Materials and Methods

PATIENT POPULATION

This retrospective study included one hundred consecutive patients (60 females, 40 males; mean age: 48 years, 95% CI: 45.1–50.9) with known or suspected pudendal neuropathy who underwent MR neurography at the Diagnostic Center of Affidea Iniziativa Medica, Monselice (Padua), Italy, between January and May 2024. According to the Nantes criteria[13] inclusion criteria comprised pain in the pudendal nerve territory, symptom exacerbation while sitting, absence of nocturnal pain causing awakening, and no objective sensory system damage on clinical examination. A positive response to pudendal nerve block was inconsistently reported.Additional symptoms included burning, shooting pain, numbness, allodynia, dyspareunia, intolerance to vulval contact, rectal or vaginal foreign body sensation, pain during defecation, and tenderness on palpation of the ischial spine. Exclusion criteria included coccygeal, gluteal, or pubic pain, pruritus, and proctalgia fugax.

STUDY PROTOCOL

A standardized MR neurography protocol[14] developed over 13 years and 1,650 pelvic MR examinations has been updated and applied to the imaging series of the 100 patients.

PATIENT PREPARATION

A detailed clinical history was obtained, including symptom onset, duration, location, radiation, triggering and relieving factors, and associations with urinary, sexual, and bowel functions. Previous treatments and diagnostic findings were reviewed. Patients were informed about the procedure duration (~45 minutes), the importance of remaining still, and the absence of contrast agents or invasive maneuvers. Cardiac gating was performed using a fingertip pulse oximeter. Patients were asked to empty their bladder before scanning.

EQUIPMENT

MR imaging was performed using a 1.5T superconductive scanner (Philips Multiva Galaxy, Netherlands) with a 16-channel SENSE torso phased-array coil. Key specifications included:

- Gradient amplitude: 33 mT/m
- Slew rate: 120 mT/m/ms
- Rise time: 0.27 ms
- Gradient field distribution: max dB/dT 73 T/s
- Cardiac gating: Li-Polymer pulse oximeter (Invivo, USA)

IMAGE ACQUISITION

The protocol consisted of two phases, first the anatomical and then the neurographic one (Table 1):

Table 1. *Technical settings for MR neurography protocol of the pudendal nerve.*

Phase	Anatomic Phase					Neurographic Phase		
Series	**Series 1**	**Series 2**	**Series 3**	**Series 4**	**Series 5**	**Series 6**	**Series 7**	**Series 8**
Pulse sequence	TSE T2-W	TSE T2-W	TSE T2-W	TSE T2-W	TSE T2-W	PD SPAIR BB	PD SPAIR BB	PD SPAIR BB
Scan plane	Sagittal	Coronal	Axial	Axial oblique	Coronal oblique	Coronal	Coronal oblique	Axial oblique
FOV (mm)	380	450	450	482	484	310	311	420
Rec Matrix	576	576	576	576	576	704	720	560
Slice thick/ gap (mm)	3.2 / 0.4	3.2 / 0.4	4 / 0.4	4 / 0.4	4 / 0.4	4 / 0.4	3.5/ 0.3	3.5/ 0.35
Flip angle (°)	90	90	90	90	90	90	90	90
Scan time (min/sec)	3:44	3:00	3:37	2:55	2:59	6:40	3:20	5:20
Slices (n°)	84	52	56	24	25	42	20	32
TR (ms)	5425	5739	5670	3000	3000	1905	2000	2000
TE (ms)	100	100	100	100	100	40	40	40
Inv delay (ms)						100	100	100
NEX	3	3	4	3	3	1	1	1
BB inv Delay						608.5	624.2	624.2
Entered heartrate						63	60	60
Max heart phases						5	5	5
TSE factor	27	23	23	23	23	25	25	28

Note: TSE = Turbo Spin Echo; PD = Proton Density; SPAIR = Spectral Adiabatic Inversion Recovery; BB = Black Blood; FOV = Field of View; NEX = Number of Excitations; TR = Repetition Time; TE = Echo Time.

- **Phase 1**: T2-weighted turbo spin echo sequences in sagittal, axial, coronal and oblique planes for anatomical assessment.
    - Sagittal: TR/TE 5426/100 ms, thickness 4 mm, gap 3 mm, matrix 256×347, FOV 281 mm, scan time 06:52
    - Axial: TR/TE 5661/100 ms, thickness 4 mm, gap 3 mm, matrix 364×417, FOV 292 mm, scan time 02:49
    - Coronal: TR/TE 5739/100 ms, thickness 3 mm, gap 3 mm, matrix 452×429, FOV 450 mm, scan time 04:24
- **Phase 2**: Proton density SPAIR sequences with fat and flow suppression (black blood technique) in coronal and oblique planes.
    - Coronal SPAIR: TR/TE 1905/40 ms, inversion delay 608.5 ms, matrix 232×247, thickness 4 mm, gap 4 mm, 42 slices, scan time 06:40

The pudendal nerve was visualized from its origin at the S2–S4 sacral foramina through the Alcock canal to its terminal branches.

IMAGE ANALYSIS

Images were analyzed side-by-side, focusing on the four anatomical sites prone to pudendal nerve entrapment:

1. Sciatic notch (piriformis muscle)
2. Ischial spine and sacrotuberous ligament
3. Alcock canal (obturator internus muscle)
4. Distal branches (dorsal penile/clitoral nerves)

In cases of injury, the pudendal nerve appeared as a *hyperintense linear structure* on DP SPAIR double IR BB sequences. Coronal oblique views were optimal for visualizing the nerve's exit and re-entry near the ischial spine, while axial oblique views best depicted its course through Alcock's canal.

Additional diagnostic criteria included:

- Architectural distortion, deviation, caliber changes, and perineural fibrosis
- Loss of fascicular striation (longitudinal) or honeycomb pattern (axial)
- Irregular contours and abrupt caliber changes (entrapment neuropathy)
- Fat plane obliteration (perineural fibrosis)
- Onion-bulb appearance (chronic demyelinating polyneuropathy)

GRADING SYSTEM

A 0–3 point brightness visual scale (B-scale) was developed to grade pudendal nerve injury within the Alcock's canal (Figure 1) by comparing its signal intensity on axial DP SPAIR double IR BB images to that of static intravescical fluid, where 0 = no hyperintensity (no injury); 1 = barely visible hyperintensity (mild injury); 2 = clearly visible hyperintensity (moderate injury); and 3= maximum intensity, equal to that of tissues containing static fluid (severe injury).

Two radiologists (MF and TM), not specialized in peripheral neuropathies, and blinded to clinical data, independently reviewed the images to assign the score. Discrepancies were resolved by a third expert reader (VP).

STATISTICAL ANALYSIS

Statistical analysis was performed using MedCalc software (version 14.8.1; MedCalc Software Ltd., Ostend, Belgium). Continuous variables were expressed as mean ± standard deviation (SD) and 95% confidence intervals (CI), while categorical data were presented as absolute numbers and percentages. Inter- and intra-observer agreement for the visual grading scale (B-scale) was assessed using weighted kappa (WK) statistics, with corresponding standard errors (SE) and 95% CI values. A p-value < 0.05 was considered statistically significant.

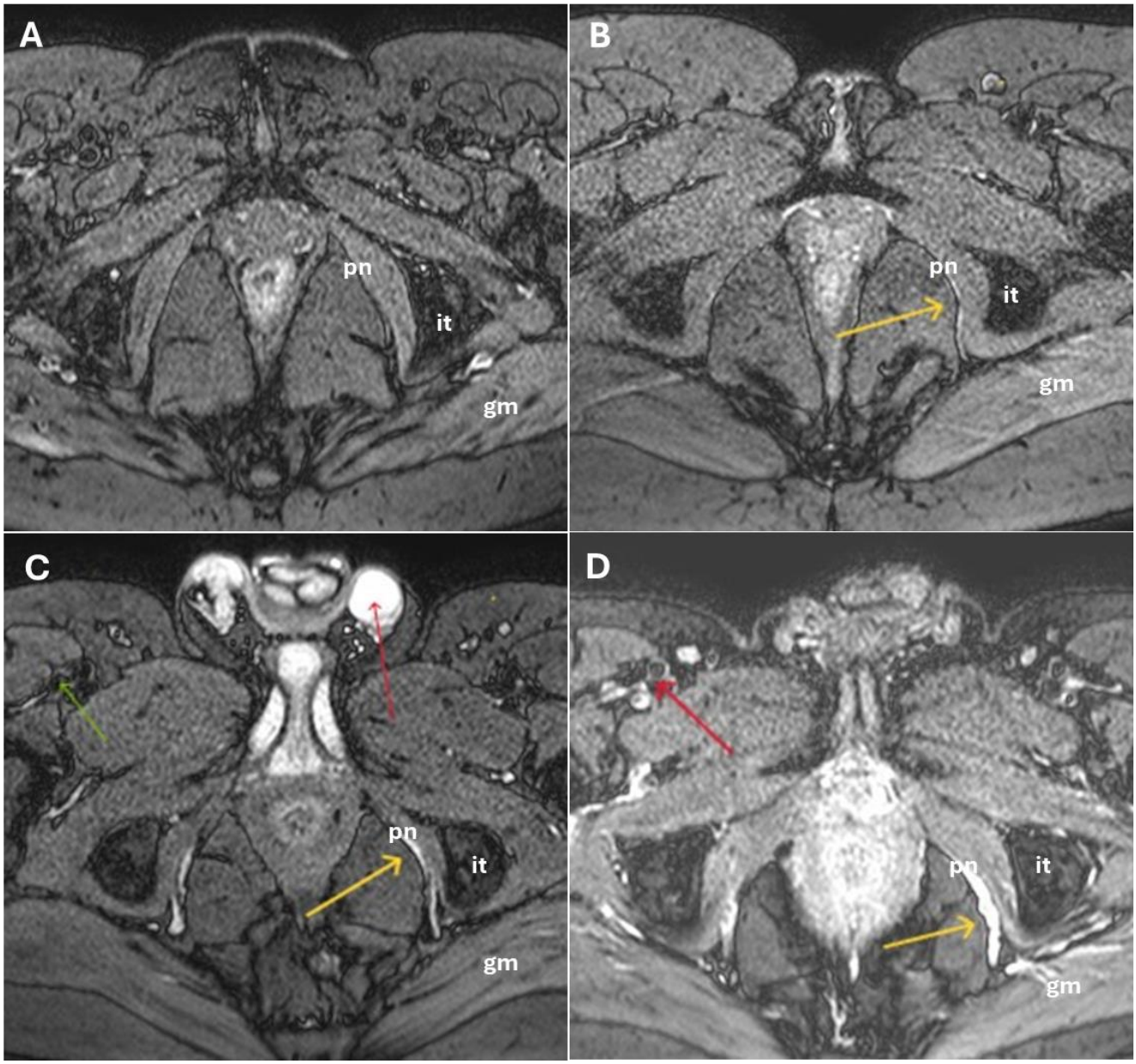

Figure 1. Grading of pudendal nerve signal brightness on axial oblique BB images, using stationary fluid (thin red arrow) and flow suppression (thick red arrow) as references. **Upper panel (a–b)**: Grade 0, no hyperintensity; Grade 1, minimal increase. **Lower panel (c–d)**: Grade 2, clear increase not equal to fluid; Grade 3, marked increase with nerve enlargement. Abbreviations: pn, pudendal nerve; it, ischiatic tuberosity; gm, gluteus maximus.

Results

CLINICAL FINDINGS

Females were slightly older than males (mean ± SD: 50.1 ± 15.3 vs. 44.8 ± 12.4 years). During history taking, 21 female patients reported episodes of sexual abuse. Trauma to the sacrococcygeal region or pelvic floor—either recent or past—was more frequently observed in women, as was a history of prior surgery (39 vs. 28 and 35 vs. 7 cases, respectively). The average time interval between symptom onset and diagnosis was 5 ± 1.3 years in men and 8 ± 3.1 years in women. The most frequent symptoms in males included pain in the external genitalia (32 cases) and pain during ejaculation (12 cases). In females, vulvodynia (51 cases) and pain during intercourse (49 cases) were predominant. Lower urinary tract symptoms (LUTS) included voiding dysfunctions (31 cases in men vs. 18 in women) and recurrent episodes of prostatitis or cystitis (38 vs. 47 cases in males and females, respectively). A complete summary of the characteristics of the study population is presented in Table 2.

Table 2. *Epidemiologic data by gender, presenting symptoms, and time interval (TI) before diagnosis in the study population (n = 100).*

Item	Male (n°= 40)		Female (n°= 60)	
	n°	%	n°	%
Age (yrs)				
Mean ± SD	44.4 ±12.4	/	50.1 ±15.3	/
Range	21-67	/	21-75	/
History				
Trauma	28	70	39	65
Prior pelvic surgery	7	17.5	35	58.3
Sexual abuse	/	/	21	35
Symptoms				
Pain at intercourse	9	22.5	49	81.6
" arousal	/	/	14	23.3
" ejaculation	12	30	/	/
" ext genitalia	32	80	51	85
Associated Sympt.				
LUTs				
Recurrent cistitis	5	12.5	47	78.3
Voiding dysfunctions	31	77.5	18	30
Prostatitis	38	95	/	/
GUTs				
Dyssynergia/ODS	18	45	38	63.3
Diarrhea/constipation	8	20	24	40
TI (yrs)				
Mean ± SD	5 ± 1.3	/	8 ± 3.1	/
Range	2-8	/	4-15	/

Note: LUTS = Lower Urinary Tract Symptoms; GUTS = Bowel Rhythm Symptoms; ODS = Obstructed Defecation Syndrome; TI = Time interval between symptom onset and diagnosis.

MR FINDINGS

MR neurography was successfully performed in all 100 patients using the described 1.5T protocol. Image quality was deemed sufficient for diagnostic interpretation in 96% of cases by both Observer 1 and Observer 2. The pudendal nerve was consistently visualized in cases of damage, appearing as a hyperintense linear structure on DP SPAIR BB images along its course (Figure 2) from the sacral foramina to its terminal branches within Alcock's canal, without the need for contrast administration.

Using the 0–3 point brightness visual scale (B-scale), the distribution of correct and coincident diagnoses assessed by both observers with regard to presence and severity of nerve injury was as follows:

- Grade 0: 13 cases
- Grade 1: 33 cases
- Grade 2: 37 cases
- Grade 3: 17 cases

Intra-observer agreement was high:

- Observer 1: WK = 0.875 (SE: 0.035; 95% CI: 0.807–0.943)
- Observer 2: WK = 0.920 (SE: 0.026; 95% CI: 0.868–0.971)

Inter-observer agreement was also substantial (WK = 0.78; SE: 0.041; 95% CI: 0.70–0.85). Overall, 30 cases showed inter-rater disagreement between Observers 1 and 2, which were subsequently resolved by Observer 3 (Figure 3). Of these, 27 cases exhibited a discrepancy of only one point on the rating scale (8 cases between scores 0 and 1; 11 cases between 1 and 2; 8 cases between 2 and 3), while 3 cases showed a two-point discrepancy.

In summary, the third expert reader (Observer 3) disagreed with both non-specialized radiologists in 3 out of 100 cases, and with only one of the two in 15 cases.

Signal abnormalities were most frequently observed at the level of the ischial spine (see Figure 2) and Alcock's canal, consistent with known anatomical entrapment sites. Additional findings included architectural distortion, nerve thickening, and obliteration of perineural fat planes—features indicative of chronic neuropathic changes.

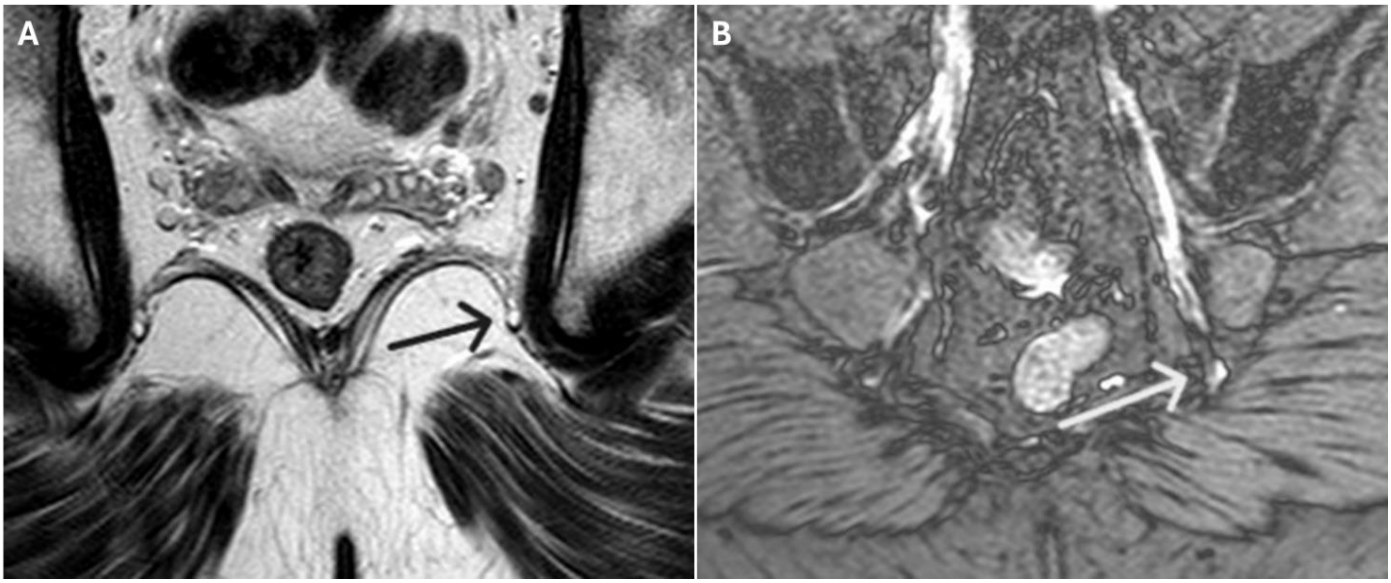

Figure 2. Grade 2 pudendal neuropathy at the nerve's entry into Alcock's canal. MR neurography, coronal oblique view: Side-by-side comparison of TSE T2-weighted image (a) and double IR BB sequence (b) shows clear identification of the pudendal nerve in end-on view (arrows), with hyperintense signal just below the ischial spine, unobscured by overlapping structures.

Figure 3. Example of Grade 1 pudendal neuropathy (yellow arrow), initially misclassified as Grade 0. Axial oblique PD_SPAIR double IR BB MR neurography reveals subtle increase in pudendal nerve signal intensity.

Discussion

The term *pudendal neuralgia* is commonly used to describe a constellation of sensory and motor symptoms affecting the saddle region—located between the anus, coccyx, and external genitalia—an area innervated by the pudendal nerve. Symptoms may extend to the pubic region, inner thighs, and buttocks, and are primarily characterized by pain while sitting, cutaneous and genital hypersensitivity, and hypertonicity of the pelvic floor musculature. First described by Amarenco et al. in 1987[15], pudendal neuralgia is now considered a subset of the broader chronic pelvic pain syndrome, resulting from pudendal nerve injury. A formal definition of the syndrome was established by a multidisciplinary working group during a 2006 meeting in Nantes, France[13], where the minimum clinical criteria for a diagnostic hypothesis were outlined.

Among the etiologies, pudendal nerve entrapment [16,17] at one of four anatomical sites is particularly significant: (a) at the piriformis muscle in the sciatic notch (Type 1); (b) at the ischial spine and sacrotuberous ligament (Type 2); (c) within Alcock's canal along the medial surface of the obturator internus muscle (Type 3); and (d) distal to the urogenital diaphragm at the peripheral branches of the dorsal penile or clitoral nerves (Type 4). Other potential causes include post-herpetic, stretch-induced, or post-radiotherapy neuropathy; neoplastic compression or direct trauma; congenital or acquired peripheral polyneuropathies; and iatrogenic injury during surgery. Although a detailed discussion is beyond the scope of this article, it is helpful to be familiar with the fundamental pathological processes underlying peripheral neuropathy, including Wallerian degeneration, axonal disintegration, and the regenerative response to nerve injury. Readers interested in a comprehensive overview are referred to the seminal review by Gaudet et al., published in 2011[18].

Until recently, imaging played a limited role in diagnosis, which remained largely clinical and empirical, based on the Nantes criteria and the Oswestry Disability Index[19] to assess the impact of

pain on daily functioning. Among instrumental assessments, electroneurophysiological tests—such as electromyography, somatosensory evoked potentials, cortical stimulation, and sacral reflex arc studies—have been employed. However, these tests are not universally available, and their interpretation lacks standardization. Moreover, their diagnostic accuracy may vary due to differing sensitivities in detecting lesions of large-diameter motor versus small-diameter sensory fibers.

Regarding imaging, high-resolution ultrasound using transperineal or transgluteal approaches with broadband 17–5 MHz linear-array transducers and color Doppler has been reported[20-22] to enable visualization of the fascicular echotexture and nerve density of the pudendal nerve, including differentiation from small vessels via cross-sectional area analysis. However, the authors acknowledge that routine sonographic imaging is limited by the deep anatomical location of the pudendal nerve and the steep learning curve required for accurate assessment by moderately experienced sonographers.

As an alternative, MR neurography has been available since 1992 and has evolved into a widely accessible technique for in vivo visualization of peripheral nerves and diagnosis of pudendal nerve injury. Using phased-array coils and a combination of T2-weighted fast spin-echo fat-suppressed sequences (via chemical shift selection or inversion recovery) with T1-weighted images in planes aligned with the nerve's long axis, both longitudinal and cross-sectional fascicular patterns can be clearly depicted. This approach enables differentiation between perineural and intraneural masses, identification of nerve discontinuity in severe trauma, and detection of increased nerve diameter and signal hyperintensity associated with injury. Specifically, intraneural edema, fibrosis, or other abnormalities that disrupt fascicular architecture and increase perifascicular tissue (e.g., connective tissue, blood, lymphatic vessels) contribute to the observed signal changes.

In their seminal work, Chhabra et al.[23] demonstrated that combining axial and coronal imaging with oblique sagittal reconstructions and spectral adiabatic inversion recovery (SPAIR) sequences effectively visualizes the major proximal segments of the pudendal nerve. Additionally, 3D isotropic diffusion-weighted (DW) sequences were found to better reveal fascicular structures due to superior fat and vascular signal suppression. However, the authors noted that smaller pudendal branches remained difficult to visualize across all sequences.

A notable advancement was introduced by Tagliafico et al.[24], who proposed the fascicular ratio (FR) as a novel parameter to quantify peripheral nerve injury by assessing the proportion of fascicular to non-fascicular intraneural tissue. Nevertheless, the method requires sophisticated auxiliary equipment, limiting its routine clinical applicability. More recently, Jung et al.[25] emphasized the importance of selecting MR pulse sequences that optimize homogeneous suppression of fat and blood flow in small vessels to enhance nerve signal detection.

Currently, the recommended MR neurography protocol for evaluating pudendal nerve injury includes fast 2D spin-echo sequences followed by 3D post-contrast imaging using a 3T magnet with multiplanar reconstruction. Diffusion-weighted imaging (DWI) and diffusion tensor imaging (DTI) techniques have also emerged as valuable tools for assessing the microscopic and functional properties of nerves.

Whatever the protocol, however, what is common to all is the need to consider the so-called "magic angle effect" in MR neurography as a source of diagnostic confusion in producing spurious signal hyperintensity of peripheral nerves which simulate disease. As is known, it consists in the possibility that the signal intensity of the nerve increases when the orientation of nerve fibers relative to that of the constant magnetic induction field (B_0) is close to 55°. As clearly explained by Chappel et al[26] in their valuable article, signal intensity within the nerves closely reflects that of highly ordered linearly oriented collagen: it may be that any increase in the free water within the nerve that is not so closely bound to

collagen or a loss of order within collagen and even loss of collagen itself, lead to signal hyperintensity. In addition, it should not be gorgotten that peripheral nerves are often small and have undulating courses making it difficult recognizing magic angle effect. To avoid the magic angle effect in MR neurography, radiologists have been suggested to use imaging sequences with longer echo times (TE), particularly beyond 38 ms, such as T2-weighted or T2-fat-saturated sequences as the artifact only appears in short TE sequences like T1 and gradient echo (GRE). Additional strategies include increasing the number of slices or matrix size and using fat suppression techniques. Other methods include using smaller voxel sizes, an anterior-to-posterior frequency-encoding direction, and STIR sequences, though this may not always be effective.

To our knowledge, this is the first report describing a method to isolate and visualize the pudendal nerve—akin to a vessel in a subtraction angiogram—using conventional 1.5T equipment and without contrast agents. This is achieved through a specific pulse sequence that simultaneously suppresses flow and fat signals, enabling clear differentiation between vessels and nerves within Alcock's canal, where they course in close proximity. The rationale for selecting the Black Blood (BB) pulse sequence[27] lies in its ability to suppress signal from flowing blood in the pudendal vessels, thereby enhancing the visibility of stationary fluid within the damaged nerve. This requires synchronization of image acquisition with the cardiac cycle (cardiac gating) using ECG monitoring to capture data at consistent points between successive R-waves. Additionally, a double inversion recovery (DIR) 180-degree preparation pulse nulls the signal from flowing blood as it enters the region of interest, while also suppressing fat signal and preserving the visibility of stationary structures. Consequently, any signal increase within Alcock's canal can be confidently attributed to the pudendal nerve.

This study demonstrates that MR neurography of the pudendal nerve can be effectively performed using a conventional 1.5T scanner without contrast agents. The described protocol enables consistent visualization of the nerve and its anatomical context, even in the complex pelvic region. Notably, the introduction of a visual grading scale (B-scale) offers a reproducible method for assessing nerve injury severity, as evidenced by the high inter- and intra-observer agreement achieved by two non-specialized radiologists with a short learning curve. This supports the potential for broader clinical adoption, particularly in settings with limited access to advanced imaging technology or specialized expertise. The large number of MR neurography exams (Table 3) performed at our institution between 2012 and 2025—totaling 1,560 scans—and the growing number of referrals from various specialists (urologists, gynecologists, proctologists, physiatrists, neurologists, orthopedic surgeons, anesthesiologists, and pain therapists) further support the reliability of this method. The observed nerve hyperintensity appears to be a direct indicator of pudendal neuropathy.

However, several limitations of this study should be acknowledged. First, there was no systematic correlation between imaging findings and severity of patients' presenting symptoms, as this was beyond the scope of the current investigation. Second, the study lacks a comparison with neurophysiological conduction test results. This limitation is partly due to the limited availability of such tests in our cohort (20 out of 100), rendering statistical comparison unfeasible. Both aspects are currently being addressed in ongoing studies.

Finally, a brief note is warranted to justify the Authors' decision to retrospectively select cases from early 2024 rather than from the more recent 2025 period. This choice was driven by two main considerations: (1) to ensure, by the end of 2025, a sample size equivalent to that previously analyzed, enabling a direct comparison in terms of diagnostic confidence and potential improvements following technical refinements introduced in the interim; and (2) to allow a sufficient follow-up window (two years) for personalized telephone interviews to the patient population aimed at assessing (a) the impact

of the pudendal neuropathy diagnosis—obtained through the described method—on therapeutic decisions and disease progression, and (b) the rate at which cases previously deemed negative using alternative MR neurography protocols were reclassified as positive with the current approach. In perspective, these objectives will serve to evaluate both the clinical utility and the diagnostic superiority of the proposed method over existing techniques.

Table 3. *Annual trend of MR examinations at Affidea Diagnostic Imaging Center (2012–2025).*

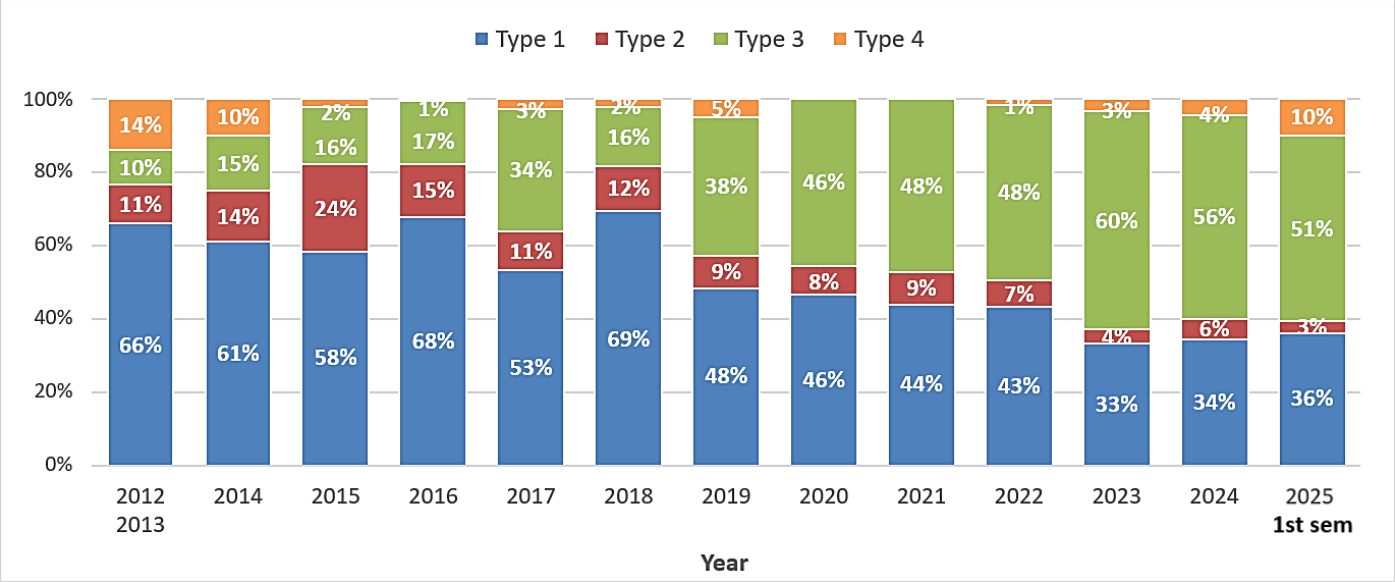

Note: Type 1 = MR Defecography Type 2 = MR Fistulography Type 3 = MR Neurography Type 4 = Mixed protocols. Since 2021, MR neurography has consistently ranked first among requested exams (≈60%). Due to limited volume, data from 2012 and 2013 were combined. Data for 2025 refer to the first semester only.

Conclusion

Regardless of the etiology, the primary evidence of pudendal nerve damage at MR neurography is signal hyperintensity along Alcock's canal. This sign, however, has diagnostic value only after ruling out other potential confounding sources, namely vessels. Fluid-sensitive and fat-suppressed sequences, as well as DWI and DTI, have proven insufficient on their own. Conversely, as shown in the current study, double IR BB pulse sequences allow confident identification of nerve damage without requiring contrast agents, advanced technology, or extensive training.

It is possible to conclude that MR neurography using a 1.5T scanner and optimized protocols with BB pulse sequences, is a reliable and accessible method for evaluating pudendal neuropathy—even by non-experienced examiners. In addition, the proposed visual grading scale for pudendal damage enhances diagnostic consistency and may facilitate standardized reporting across institutions. Our findings confirm that the most common sites of pudendal nerve entrapment are near the ischial spine and within Alcock's canal. These results are consistent with previous studies using 3T systems and contrast-enhanced techniques, suggesting that high-quality diagnostic imaging is achievable also with 1.5T systems. This approach offers a practical solution for centers without access to advanced imaging platforms, thereby expanding the availability of pelvic nerve assessment in routine clinical practice. **These findings support the clinical value of 1.5T MR neurography and encourage further multicenter studies to validate its integration into standardized diagnostic pathways.**

Disclosure:

Authors declare no conflict of interest

References:

1. Howe FA, Filler AG, Bell BA, Griffiths JR. Magnetic resonance neurography. Magn Reson Med. 1992; 28:328–38.

2. Filler AG, Howe FA, Hayes CE, Kliot M, Winn HR, Bell BA, Griffiths JR, Tsuruda JS. Magnetic resonance neurography. Lancet. 1993;341:659–61.

3. Filler AG, Kliot M, Howe FA, Hayes CE, Saunders DE, Goodkin R, Bell BA, Winn HR, Griffiths JR, Tsuruda JS. Application of magnetic resonance neurography in the evaluation of patients with peripheral nerve pathology. J Neurosurg. 1996;85 (2):299–309.

4. Maravilla KR, Bowen BC. Imaging of the peripheral nervous system: evaluation of peripheral neuropathy and plexopathy. AJNR Am J Neuroradiol. 1998;19(6):1011–23.

5. Filler A. Diagnosis and treatment of pudendal nerve entrapment syndrome subtypes: imaging, injections, and minimal access surgery. Neurosurg Focus. 2009;26(2):E9.

6. Thawait SK, Chaundhry V, Thawait GK, Wang KC, Belzberg A, Carrino JA. High-resolution MR neurography of diffuse peripheral nerve lesions. AJNR Am J Neuroradiol. 2011;32:1365–72.

7. Ohana M, Mosser T, Moussaoui A, Kremer S, Carlier RY, Lieverneaux P, Dietemann JL. Current and future imaging of the peripheral nervous system. Diagn Interv Imaging. 2014;95:17–26.

8. Wadhwa V, Hamid AS, Kumar Y, Scott KM, Chhabra A. Pudendal nerve and branch neuropathy: magnetic resonance neurography evaluation. Acta Radiol. 2017;58(6):726–33.

9. Weissman E, Boothe E, Wadhwa V, Scott KM, Chhabra A. Magnetic resonance neurography of the pelvic nerves. Semin Ultrasound CT MR. 2017; 38:269–78.

10. Soldatos T, Andreisek G, Thawait GK, Guggenberger R, Williams EH, Carrino JA, Chhabra A. High-resolution 3-T MR neurography of the lumbosacral plexus. Radiographics. 2013;33: 967–87.

11. Tagliafico AS. Peripheral nerve imaging: not only cross-sectional area. World J Radiol. 2016;8 (8):726–8.

12. Noguerol TM, Barousse R, Socolovsky M, Luna A. Quantitative magnetic resonance neurography for evaluation of peripheral nerves and plexus injuries. Quant Imaging Med Surg. 2017;7(4):398–421.

13. Labat JJ, Riant T, Robert R, Amarenco G, Lefaucheur JP, Rigaud J. Diagnostic criteria for pudendal neuralgia by pudendal nerve entrapment (Nantes Criteria). Neurourol Urodyn. 2008;27:306–10.

14. Piloni V, Bergamasco M, Chiapperin A, Mazzucco M, Felici T, Andreatini J, Nucera N, Freddi E. Magnetic resonance imaging of pudendal nerve: technique and results. Pelviperineology. 2020;39 (4):134–9.

15. Amarenco G, Lanoe Y, Perrigot M, Goudal H. Un nouveau syndrome canalaire: la compression du nerf pudendal dans le canal d'Alcock ou paralysie périnéale du cycliste. Presse Med. 1987;16(8):399.

16. Hruby S, Ebmer J, Dellon AL, Aszmann OC. Anatomy of pudendal nerve at urogenital diaphragm – new critical site for nerve entrapment. Urology. 2005;66:949–52.

17. Petchprapa CN, Rosenberg ZS, Sconfienza LM, Cavalcanti CFA, La Rocca Vieira R, Zember JS. MR imaging of entrapment neuropathies of the lower extremity. Part 1. The Pelvis and Hip Radiographics. 2010;30:983–1000.

18. Gaudet AD, Popovich PG, Ramer MS. Wallerian degeneration: gaining perspective on inflammatory events after peripheral nerve injury. Journal of Neuroinflammation. 2011; 8:110

19. Fairbank JCT, Pynsent PB. The Oswestry Disability Index. Spine. 2000;25(22):2940–53.

20. Tagliafico A, Perez MM, Martinoli C. High-resolution ultrasound of the pudendal nerve: normal anatomy. Muscle Nerve. 2013;47:403–8.

21. Pham M, Baumer T, Bendszus M. Peripheral nerves and plexus: imaging by MR-neurography and high-resolution ultrasound. Curr Opin Neurol. 2014;27(4):370–9.

22. Moller I, Miguel M, Bong DA, Zaottini F, Martinoli C. The peripheral nerves: update on ultrasound and magnetic resonance imaging. Clin Exp Rheumatol. 2018;36(114):145–58.

23. Chhabra A, McKenna CA, Wadhwa V, Thawait GK, Carrino JA, Lees GP, Dellon AL. 3T magnetic resonance neurography of pudendal nerve with cadaveric dissection correlation. World J Radiol. 2016;8(7):700–6.

24. Tagliafico AS, Tagliafico G. Fascicular ratio: a new parameter to evaluate peripheral nerve pathology on magnetic resonance imaging. Medicine (Baltimore). 2014;93(14):e68.

25. Jung JY, Lin Y, Carrino JA. An updated review of magnetic resonance neurography for plexus imaging. Korean J Radiol. 2023;24(11):1114–30.

26. Chappel KE, Robson MD, Stonebridge-Foster A, Glover A, Allsop JM, Williams AD, Herlihy AH, Moss J, Gishen P, Bydder GM. Magic angle effect in MR neurography. Am J Neuroradiol. 2004; 25: 431-440.

27. Henningsson M, Malik S, Botnar R, Castellanos D, Hussain T, Leiner T. Black-Blood contrast in cardiovascular MRI. J Magn Reson Imaging. 2022; 55:61–80.

